LBL-19828
c.2

Lawrence Berkeley Laboratory
UNIVERSITY OF CALIFORNIA

Materials & Molecular Research Division

Invited talk presented at the ASTM 18th National Symposium on Fracture Mechanics, Boulder, CO, June 25-27, 1985

RECEIVED
LAWRENCE
BERKELEY LABORATORY

NOV 15 1985

LIBRARY AND
DOCUMENTS SECTION

A COMPARISON OF FATIGUE CRACK PROPAGATION IN MODES I AND III

R.O. Ritchie

June 1985

TWO-WEEK LOAN COPY

This is a Library Circulating Copy
which may be borrowed for two weeks.

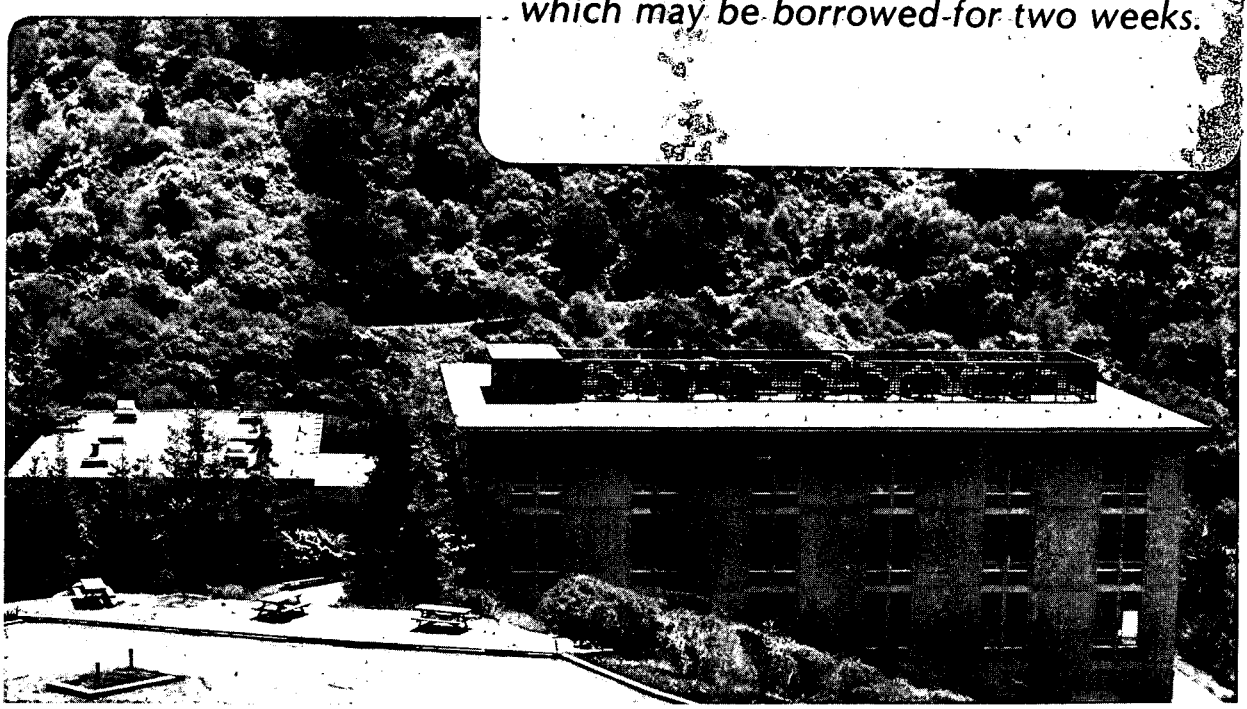

Prepared for the U.S. Department of Energy under Contract DE-AC03-76SF00098

LBL-19828
c.2

DISCLAIMER

This document was prepared as an account of work sponsored by the United States Government. While this document is believed to contain correct information, neither the United States Government nor any agency thereof, nor the Regents of the University of California, nor any of their employees, makes any warranty, express or implied, or assumes any legal responsibility for the accuracy, completeness, or usefulness of any information, apparatus, product, or process disclosed, or represents that its use would not infringe privately owned rights. Reference herein to any specific commercial product, process, or service by its trade name, trademark, manufacturer, or otherwise, does not necessarily constitute or imply its endorsement, recommendation, or favoring by the United States Government or any agency thereof, or the Regents of the University of California. The views and opinions of authors expressed herein do not necessarily state or reflect those of the United States Government or any agency thereof or the Regents of the University of California.

LBL-19828

A COMPARISON OF FATIGUE CRACK PROPAGATION IN MODES I AND III

R. O. Ritchie

Materials and Molecular Research Division,
Lawrence Berkeley Laboratory,
and
Department of Materials Science and Mineral Engineering,
University of California, Berkeley, CA 94720

June 1985

invited presentation at the
ASTM 18th National Symposium on Fracture Mechanics,
University of Colorado, Boulder, Colorado, 25-27 June 1985

This work was supported by the Director, Office of Energy Research, Office of Basic Energy Sciences, Materials Science Division of the U.S. Department of Energy under Contract No. DE-AC03-76SF00098.

A COMPARISON OF FATIGUE CRACK PROPAGATION IN MODES I AND III

R. O. Ritchie[1]

REFERENCE: Ritchie, R. O., **"A Comparison of Fatigue Crack Propagation in Modes I and III,"** Fracture Mechanics: Eighteenth Symposium, ASTM STP, R. P. Reed and D. T. Read, Eds., American Society for Testing and Materials, Philadelphia, PA, 1985.

ABSTRACT: The propagation behavior of fatigue cracks in Mode III (anti-plane shear), measured under cyclic torsion, is described and compared with more commonly encountered behavior under Mode I (tensile opening) loads. It is shown that a unique, global characterization of Mode III growth rates, akin to the Paris "law" in Mode I, is only possible if characterizating paramaters appropriate to large-scale yielding are employed and allowance is made for crack tip shielding from sliding crack surface interference (i.e., friction and abrasion) between mating fracture surfaces. Based on the crack tip stress and deformation fields for Mode III stationary cracks, the cyclic crack tip displacement, $(\Delta CTD)_{III}$, and plastic strain intensity range, $\Delta\Gamma_{III}$, have been proposed and are found to provide an adequate description of behavior in a range of steels, provided crack surface interference is minimized. The magnitude of this interference, which is somewhat analogous to crack closure in Mode I, is further examined in the light of the complex fractography of torsional fatigue failures and the question of a "fatigue threshold" for Mode III crack growth. Finally, micro-mechanical models for cyclic crack extension in anti-plane shear are briefly described, and the contrasting behavior between Mode III and Mode I cracks subjected to simple variable amplitude spectra is examined in terms of the differing role of crack tip blunting and closure in influencing shear, as opposed to tensile opening, modes of crack growth.

KEY WORDS: fatigue (materials), cracking (fracturing), crack propagation, torsion, Mode I (tensile opening), Mode III (anti-plane shear), crack closure and sliding interference, fatigue thresholds, variable amplitude loading.

---

[1]Professor of Metallurgy, Materials and Molecular Research Division, Lawrence Berkeley Laboratory, and Department of Materials Science and Mineral Engineering, University of California, Berkeley, Calif 94720.

Introduction

Over the past thirty years, there have been numerous analytical models proposed for cyclic crack extension in Mode III (anti-plane shear) (1-9),[2] presumably because of the mathematically convenient form of continuum solutions describing the local Mode III crack tip stress and deformation fields (2,10,11). In contrast, experimental studies of Mode III crack **growth** behavior are rare (3,7-9,12-21), particularly when compared to the extensive literature on the propagation behavior of fatigue cracks in Mode I (tensile opening loading) (reviewed, for example, in ref. 22). This is somewhat surprising as torsional fatigue fractures are a common mode of engineering service failures (23), particularly in the automobile industry with springs and transmission components, such as drive and prop shafts, and in the power generation industry with large turbo-generator rotors. In addition to the paucity of fracture mechanics data on Mode III crack growth rates, mechanistic aspects are also relatively unknown. As metallurgical consultant D. J. Wulpi writes in a recent article (23), "...after many years of studying and analyzing fractures, it has become obvious that the various types of torsional fractures are not well understood...."

The intent of this paper is to review what is known about the fracture mechanics and micro-mechanistic aspects of Mode III fatigue crack growth and to compare such behavior to that more commonly

---

[2]The numbers in brackets refer to the list of references appended to this paper.

encountered in Mode I. We examine first the anti-plane strain crack tip fields and the choice of appropriate characterizing parameters for crack advance, under both small-scale yielding and elastic-plastic conditions, and apply these to steady-state Mode III fatigue crack propagation. It is shown that a global characterization of growth rates in small- or large-scale yielding can be achieved in terms of the range of crack tip displacement (ΔCTD), similar to that in Mode I, although the Mode III crack extends over a far smaller proportion of the ΔCTD each cycle. As crack surfaces remain in sliding contact, this is attributed in part to the occurrence of "sliding crack surface interference" (14-16) where, analogous to crack closure in Mode I, abrasion and interlocking between asperities on mating fracture surfaces provide a potent mechanism for "shielding" the crack tip from the full applied "driving force". The significance of this interference to both the fractography of Mode III failures and the relative rates of crack growth compared to Mode I behavior is discussed in some detail. In addition, several recent models (8) for Mode III crack extension are examined and compared to torsional crack growth data in a range of steels. Finally, the sharp contrast between Mode I and Mode III crack growth behavior under variable amplitude cyclic loading is described in the light of current ideas on "damage accumulation" and fatigue crack closure.

Crack Tip Fields

For both Mode I and Mode III cracks, the stress and strain fields in the vicinity of the crack tip have been determined using asymptotic continuum mechanics analysis. For linear elastic solids in Mode I, the local singular stress field at distance r, polar angle θ, from the tip of a stationary crack is given in terms of the Mode I stress intensity factor, K_I, in the limit of $r \to 0$, as (24):

$$\sigma_{ij} \to \frac{K_I}{\sqrt{2\pi r}} \cdot f_{ij}(\theta) \quad , \tag{1}$$

whereas for elastic-plastic solids (actually non-linear elastic solids where $\bar{\varepsilon}/\varepsilon_0 = \alpha(\bar{\sigma}/\sigma_0)^n$), the local Mode I singular stress, strain and displacement fields are given in terms of the path-independent integral J (25), as $r \to 0$ (26,27):

$$\frac{\sigma_{ij}}{\sigma_0}(r,\theta) \to \left(\frac{J}{\alpha\sigma_0\varepsilon_0 I_n r}\right)^{1/(n+1)} \tilde{\sigma}_{ij}(\theta,n) \quad , \tag{2a}$$

$$\frac{\varepsilon_{ij}}{\varepsilon_0}(r,\theta) \to \alpha\left(\frac{J}{\alpha\sigma_0\varepsilon_0 I_n r}\right)^{n/(n+1)} \tilde{\varepsilon}_{ij}(\theta,n) \quad , \tag{2b}$$

$$\frac{u_i}{r}(r,\theta) \to \alpha\varepsilon_0\left(\frac{J}{\alpha\sigma_0\varepsilon_0 I_n r}\right)^{n/(n+1)} \tilde{u}_i(\theta,n) \quad , \tag{2c}$$

where σ_0 and ε_0 are the yield stress and strain, respectively, α is a material constant of order unity, f_{ij} is a dimensionless function of θ, $\tilde{\sigma}_{ij}(\theta)$, $\tilde{\varepsilon}_{ij}(\theta)$ and $\tilde{u}_i(\theta)$ are normalized stress, strain and

displacement functions of θ, and I_n is a numerical constant weakly dependent upon the strain hardening exponent n.

For Mode III anti-plane shear, the corresponding solutions for the linear elastic stationary crack are given, in the limit of $r \to 0$, by (28):

$$\sigma_{xy} = \frac{-K_{III}}{\sqrt{2\pi r}} \sin\frac{\theta}{2} \quad , \tag{3a}$$

$$\sigma_{yz} = \frac{K_{III}}{\sqrt{2\pi r}} \cos\frac{\theta}{2} \quad , \tag{3b}$$

where K_{III} is the stress intensity factor in Mode III. For the non-linear elastic crack, the singularity field can be written as (2):

$$\tau_p(r,\theta) \to \tau_o\left(\frac{r_y}{r}\right)^{1/(n+1)} \tilde{\tau}_p(\theta) \quad , \tag{4a}$$

$$\gamma_p(r,\theta) \to \gamma_o\left(\frac{r_y}{r}\right)^{n/(n+1)} \tilde{\gamma}_p(\theta) \quad , \tag{4b}$$

where τ_o and γ_o are the shear yield stress and strain, respectively, r_y is the distance from the crack tip to the elastic-plastic boundary, and $\tilde{\tau}_p(\theta)$ and $\tilde{\gamma}_p(\theta)$ are normalized shear stress and strain functions of θ. For elastic-perfectly plastic stationary cracks, the field (which exactly satisfies incremental plasticity theory) can be expressed in simplier form as (29):

$$\gamma_p = \gamma_o\left(\frac{r_y}{r}\right) \quad . \tag{5}$$

Such solutions are used to define appropriate characterizing parameters for crack extension. In Mode I, where the plastic zone size under plane strain conditions is fabiform in shape and given approximately by (30):

$$r_y \sim \frac{1}{2\pi}\left(\frac{K_I}{\sigma_o}\right)^2 \quad , \tag{6}$$

the stress intensity K_I provides characterization of the unique linear elastic crack tip field when the plastic zone is small compared to crack size. Under such small-scale yielding conditions, a crack tip (opening) displacement $(CTD)_I$ can be estimated as (30):

$$(CTD)_I \sim \frac{1}{2}\ \frac{K_I^{\,2}}{\sigma_o\ E} \quad , \tag{7}$$

where E is the elastic (Young's modulus). In the presence of more extensive plasticity, the non-linear elastic crack tip field can be characterized by the J-integral or the $(CTD)_I$.

In Mode III, where the plastic zone is circular in shape, with a diameter given by (2,29):

$$r_y \sim \frac{1}{\pi}\left(\frac{K_{III}}{\tau_o}\right)^2 \tag{8}$$

linear elastic fields can be characterized by K_{III}, with the Mode III crack tip displacement $(CTD)_{III}$ under small-scale yielding given by (2,29):

$$(CTD)_{III} \sim \frac{2}{\pi} \frac{K_{III}^2}{\tau_o G} \quad , \tag{9}$$

where G is the shear modulus. With large scale plasticity, the cyclic crack tip displacement and the **plastic strain intensity range,** $\Delta\Gamma_{III}$, have been suggested as appropriate characterizing parameters for Mode III crack extension (6). Γ_{III} is defined in terms of the radius of the plastic zone, r_y, and the Walsh and Mackenzie's solution (10) for the shear strain distribution in a circumferentially-notched cylinder of elastic-rigidly plastic material subjected to a torque M:

$$\gamma = \frac{\tau_o}{G}\left(\frac{r'}{r_p}\right)^2\left(\frac{r_N - r_p}{r_N - r'}\right) \quad , \tag{10}$$

where the radii r', r_N, and r_p are defined in Fig. 1. Although the plastic strain is infinite at the crack tip ($r' = r_N$), the parameter $(r_N - r')\gamma$ clearly is finite and defines the intensity of plastic shear strain in the crack plane. For cyclic loading, this gives (6):

$$\Delta\Gamma_{III} = \lim_{r_N - r' \to 0} [(r_N - r')\Delta\gamma] = \frac{2\tau_o}{G}\,\Delta\left[\left(\frac{r_N}{r_p}\right)^2 r_y\right] \quad . \tag{11}$$

Note that the plastic strain intensity so defined ($\Gamma_{III} = \lim[(r_N - r')\gamma]$) is analogous to the linear elastic stress intensity where $K_I = \lim[\sigma(r)\sqrt{2\pi r}]$. In the limit of small-scale yielding, where $r_N \to r_p$, the plastic strain intensity range can be related to the Mode III cyclic crack tip displacement simply by the expression:

$$(\Delta CTD)_{III} = 2\Delta\Gamma_{III} \quad . \tag{12}$$

For large-scale yielding, Eq. (12) is only approximately correct. The computation of Γ_{III} values under these conditions specifically involves determination of analytical expressions for r_y, and has been discussed in detail elsewhere (14,20 31).

Mode III Fatigue Crack Growth Behavior

The large majority of experimental research on the propagation behavior of fatigue cracks has been conducted under Mode I loading. For behavior in other modes, there have been several studies (e.g., refs. 32 - 37) on the "slant" crack loaded in tension, which experiences both Mode I and either Mode II or Mode III displacements. In general, it has been found that such cracks are unstable with respect to Mode I and hence tend to deviate to the Mode I plane (37). To obtain stable non-Mode I growth, the tensile mode must be suppressed. This has been demonstrated by Smith (36), who obtained stable Mode II crack extension of a slant crack through the application of cyclic compression, which suppresses the tensile mode by closing the crack surfaces together.

Unlike behavior in Mode II, with sufficient plasticity stable crack advance in Mode III can be readily attained. Whereas Mode I behavior commonly is measured in bending or tension, with rare exception (12) fatigue crack propagation rates in pure Mode III are determined on cylindrical bars or tubes tested in cyclic torsion

(e.g., refs. 7 -9). As the surfaces of maximum shear are perpendicular to and parallel to the axis of the cylinder, Mode III cracking can occur both longitudinally and radially (Fig. 2). For this reason, a circumferential notch generally is employed such that, provided extreme care is taken to minimize misalignment which induces undesired bending moments and hence asymmetric cracks, radially-inward concentric crack growth is Mode III in torsion and Mode I in tension. Shear crack growth, however, is promoted by extensive plasticity (7), as can be demonstrated by twisting a brittle material like a piece of chalk, which will fail by a helical fracture along plane of maximum tensile stress, compared to a ductile material like plasticene which simply will shear off. Accordingly, at low stresses, i.e., less than 70% of yield (7), Mode III crack extension becomes unstable to Mode I, with the result that torsional failures occur either macroscopically in Mode I with a helical fracture surface, locally in Mode I with 45° branch cracks, or by a combination of modes (7).

Typical crack growth data (7,8,14-20), determined by such procedures using electrical potential methods to monitor crack extension (38), are shown in Figs. 3-5. In Fig. 3, Mode III crack growth rates $(dc/dN)_{III}$ are plotted as a function of the cyclic crack tip displacement $(\Delta CTD)_{III}$ and plastic strain intensity range $(\Delta\Gamma_{III})$, under cyclic conditions of zero mean stress (R = -1), for several steels, ranging in tensile yield strength (σ_y) from 260 MPa for AISI 1018 to 956 MPa for quenched and $650^{o}C$ tempered AISI 4340

steel. Although plastic zone sizes can approach 50% of the section diameter at the higher crack tip displacements, i.e., conditions are well beyond small-scale yielding, Mode III growth rates clearly are well characterized by $(\Delta CTD)_{III}$, or $\Delta\Gamma_{III}$. Variations in behavior between the different alloys are not large, apart from the earliest published data (e.g., refs. 7 and 13) where sliding crack surface interference was not accounted for (see below).

In Fig. 4, Mode III growth rates for an A469 rotor steel (yield strength 621 MPa) are compared with corresponding Mode I rates at equivalent cyclic crack tip displacements (ΔCTD) (8). As several authors have noted previously (7-9,13,34), Mode I growth rates exceed those in Mode III when compared at equivalent ΔCTD values or stress intensity ranges. In fact, the crack growth increment in Mode III is only a small fraction (<1/100) of the crack tip displacement per cycle, consistent with micro-mechanical models (7,8). Tschegg (15,18,20) has suggested that where procedures are used to remove **completely** crack surface interference, Mode III cracks actually may grow faster than in Mode I, at least for higher growth rates above 5 x 10^{-3} mm/cycle, when compared at equivalent ΔCTD values. This, however, is a somewhat unfair comparison since the corresponding interference between crack surfaces in Mode I, i.e., crack closure, was not similarly accounted for.

As data are scarce for Mode III crack extension, the influence of various mechanical, microstructural and environmental variables are largely unknown. For example, Mode III corrosion fatigue crack

growth behavior has not been characterized to date, although certain authors have examined the problem of corrosion fatigue life in torsion using S/N tests on unnotched samples (e.g., ref. 39). In view of the widely differing hydrostatic stress states between tension and anti-plane shear, this would seem to be an important area for research, especially for environments which induce hydrogen embrittlement. Microstructural effects on Mode III crack growth also are essentially unexplored, although it is apparent that material strength has little influence on crack extension rates (Fig. 3). Limited data (8,13) are available on the role of mean stress, or load ratio R (i.e., ratio of minimum to maximum load or stress). Unlike Mode I behavior where increasing the load ratio can markedly increase growth rates due primarily to a reduced influence of crack closure at high R (40), in Mode III where there is no closure as such, load ratios effects appear insignificant, as illustrated by the R = -1 and -0.5 results (8) for the A469 rotor steel in Fig. 5. It has been noted, however, that at higher R values, e.g., $\sim$ 0.1, Mode III cracks show a tendency to become destabilized and to form Mode I branch cracks more readily, although in many cases the effect on growth rates is not that significant (13). The influence of other mechanical variables, such as cyclic frequency, wave form, and geometry, has not been examined.

Fractography

The fractography of torsional failures is complex and is associated with several distinct fracture morphologies, summarized in Fig. 6 (21). Pure Mode III cracks have flat, featureless fracture surfaces with clear signs of abrasion, i.e., evidence of fretting oxide debris and fractographic details obscured by friction and rubbing (Fig. 7a). In fact, Tschegg (18) reports the presence of black spherical Fe_3O_4 particles on torsional fracture surfaces in 4340 steel after testing and red Fe_2O_3 powder squeezing out of the crack during the test. The presence of Mode III fatigue striations also has been claimed for torsional failures in mild steel (20), although their origin is uncertain.

At lower growth rates, typically below 10^{-4} to 10^{-5} mm/cycle (7,13-16), or with the superposition of small tensile loads (7), there is an increasing tendency for secondary or branch cracks to form and deviate off the macroscopic radial Mode III plane (Fig. 7b). In certain materials, these secondary cracks are 90° longitudinal Mode III cracks which intersect the radial plane (Fig. 6d) (14). However, more commonly they are primarily intersecting Mode I branch cracks which form on complementary planes at $\pm 45^{o}$ to the radial Mode III surface, as shown in Fig. 8. This mode of failure, which is locally pure Mode I and only "nominally" Mode III in the macroscopic sense, been termed "factory-roof" fracture (41,7), and is a common type of torsional fracture found in service (23).

Factors responsible for the transition from pure radial Mode III to local Mode I factory-roof fractures (e.g., Fig. 6c) are far from understood. However, the transition is promoted at lower growth rates, with increasing crack length (7,14-16) and in larger specimen diameters (18). This can be explained qualitatively in terms of the lower "effective" ΔK_{III} or $(\Delta CTD)_{III}$ experienced at the tip, favoring Mode I separation, as the latter two factors have been shown to enhance crack tip shielding due to sliding crack surface interference from the increased fracture surface area (7,14-16,18).

It has been suggested that "true" Mode III crack growth, as evidenced by the flat, featureless surfaces in Figs. 6a and 7a, is nothing more than a local Mode I factory-roof fracture with the Mode I facets destroyed by the rubbing (34). This is unlikely, however, as "true" Mode III fractures are only observed at higher $(\Delta CTD)_{III}$ or ΔK_{III} values, where the larger plastic zones promote sufficient crack opening to minimize the abrasion between sliding crack surfaces, as discussed below.

Crack Surface Interference

As noted above, a prominant characteristic of Mode III crack extension, in fact of all non-Mode I cracking, is the rubbing together of sliding crack surfaces during cyclic loading (14-16). Aside from causing heating of the specimen and abrasion of the fracture surfaces, which obscures fractographic details and promotes fretting wear debris, this phenomenon leads problems with electrical

shorting in electrical potential crack monitoring (38), and most importantly to a marked reduction in the "effective crack tip driving force" for Mode III crack extension. The latter effect is known as **sliding crack surface interference** (14-16), or sometimes torsional or Mode III crack closure due to its somewhat analogous effect to Mode I crack closure (e.g., ref. 40) in shielding the crack tip from the full applied loads. Probable mechanisms for such interference, involving friction, abrasion, debris formation and interlocking, are illustrated in Fig. 9 and clearly enable the broken portion of the test piece to carry a portion of the applied torque. The analogy to Mode I crack closure is reasonable, particularly in the case of the oxide-induced and roughness-induced mechanisms (40), although in contrast to behavior in Mode III, Mode I closure does not act over the entire fatigue cycle (Fig. 10).

The effect of crack surface interference on Mode III growth rates can be dramatic. When cracks have been cycled at constant ΔK_{III} (14-16) or at constant $\Delta \Gamma_{III}$ (20), where fracture mechanics similitude would normally dictate constant rates of crack advance independent of crack size, growth rates are essentially non-unique and decelerate progressively by several orders of magnitude with increasing crack size. This is illustrated in Fig. 11 by torsional results (20) on mild steel (σ_y = 260 MPa). The effect can be seen to be enhanced at larger crack lengths, particularly after the transition to factory-roof fractures, but is diminished at higher

cyclic torques where the larger plastic zones permit larger crack openings.

Providing a fracture mechanics characteration of Mode III fatigue crack extension without accounting for sliding crack surface interference simply is not feasible, as demonstrated for example in ref. 14. This is because a unique growth rate cannot be associated with any **nominal** value of ΔK_{III}, $(\Delta CTD)_{III}$, or $\Delta\Gamma_{III}$. Two experimental techniques have been used to overcome this problem, both intended to yield upper bound measurements of Mode III growth rates compared to service behavior. The first of these involves extrapolation of the $(dc/dN)_{III}$ vs. crack length c curves, measured at constant nominal "driving force" (e.g., Fig. 11), to a ficticious zero crack length where no interference can be present (15,18-20). The method is somewhat artifical and involves taking several measurements at different crack sizes to obtain one $(dc/dN)_{III}$ data point, but does yield upper bound results, as shown by results (20) for mild steel in Fig. 12. The more common technique (8,9,14,21,38), however, is to superimpose a small tensile mean load onto the cyclic torsion, thereby minimizing interference by the increased crack opening. This technique also yields upper bound results (Fig. 13), and been shown to produce unique $(dc/cN)_{III}$ data over a wide range of testing conditions (8,14). Predictably, it works well where crack surfaces are not overly rough where the required Mode I mean loads are small enough such as not interfer with crack growth behavior (8,9). This required mean load, however, will

change at different growth rates (19), due to differences in crack path morphology, and can lead to an increase in Mode I branch cracks (7). Such problems are reflected in the data on mild steel shown in Fig. 14 where increasing the magnitude of the superimposed K_I during cyclic torsion at two $\Delta\Gamma_{III}$ levels does not completely remove crack surface interference (19). Moreover, at high levels of K_I, e.g., with K_I = 10.5 MPa$\sqrt{m}$ at $\Delta\Gamma_{III}$ = 0.002 mm, the trend in $(dc/dN)_{III}$ with increasing c can be seen to be changed abruptly, presumably arising from enhanced surface interference from an increased propensity of Mode I branch cracks.

Sliding crack surface interference also has been studied analytically. By assuming that the fracture surface asperities compel the crack faces to separate, thereby causing a normal force which in turn generates a frictional force that acts in opposition to the applied torque, Gross (42) has recently estimated the torque lost to fraction, M_f, in terms of friction coefficient μ, asperity height t, crack size c, and ligament size r_N, viz:

$$M_f = \frac{\mu G t}{(1-\nu)} \left[\frac{c^2}{2} - 2cr_N + r^2 \ln\left(\frac{c}{t}\right)\right] \quad , \qquad (13)$$

where G is the shear modulus and ν is Poisson's ratio. By reducing the applied torque by M_f, computed using asperity heights between 100 and 200 μm, Eq. (13) has been shown to provide reasonable predictions of the progressive decay in growth rates, as depicted in Fig. 11 (42).

Behavior under Cyclic Mode I with Steady Mode III

Analogous to the studies described above on the influence of steady Mode I loading superimposed on cyclic Mode III (7,21), several authors (41,43) have examined the influence of steady Mode III superimposed on cyclic Mode I. Whereas in the former instance, the superimposed Mode I load can lead to faster Mode III growth rates by limiting crack surface interference by opening the crack, results for superimposing a Mode III load on cyclic Mode I invariably show Mode I growth rates to be decreased progressively with increasing K_{III}. This is shown for a Ti-5Al-2.5Sn alloy (σ_y = 760 MPa) in Fig. 15 (41). Similar behavior has been reported in steels (43).

In all cases, the decrease in growth rates (typically by two orders of magnitude) is concurrent with a marked change in crack path morphology from being relative linear to a zig-zag profile characteristic of a factory-roof fracture. Accordingly, one would reason that the reduction in Mode I growth rates with superimposed Mode III results principally from a reduced "effective driving force" actually experienced at the crack tip, i.e., a lower local stress intensity range, due to crack deflection from the Mode I plane and the resulting roughness-induced crack closure. Similar effects are seen under (nominal) pure Mode I loading where the promotion of crack path meandering, either by crystallographic deflection (44-46) or deflection at hard phases (47), can lead to major reductions in crack growth rates.

"Thresholds" for Crack Growth

Extensive information is now available, for a wide range of materials and testing conditions, on values of Mode I fatigue thresholds, ΔK_{Ith}, below which tensile cracks are assumed to remain dormant (e.g., refs. 22,40). Furthermore, the existence of a Mode I threshold has been related mechanistically to the magnitude of crack closure generated along the crack flanks (e.g., refs. 48,49). Corresponding understanding of the Mode III threshold, ΔK_{IIIth}, is far less advanced. The majority of data has been reported by Pook and co-workers (34,35,37) who define the value of ΔK_{IIIth} in terms of the stress intensity to initiate crack growth from a torsionally-loaded circumferential crack. This can be questioned as a true Mode III threshold for crack advance in shear, however, as cracking does not commence in Mode III. The measured threshold instead represents the value of ΔK_{III} at which a Mode I branch crack initiates from the Mode III pre-crack, consistent with crack deflection calculations which accurately predict that the measured Mode III thresholds should be a factor of 1.35 larger than corresponding values in Mode I (35).

Ideally, a threshold for crack growth should be defined under conditions of decreasing "driving force" until crack growth arrests, as is commonly employed in Mode I testing (22). If this is adopted in Mode III, at low values of ΔK_{III} the Mode III cracking mode changes to a local Mode I (factory-roof) fracture long before crack arrest can occur (e.g., refs. 7, 13). Accordingly, several authors

(13,18) have defined the Mode III threshold in terms of this Mode III/Mode I transition rather than in terms of the cessation of cracking. Values of ΔK_{IIIth} defined in this way, however, are not comparable with crack arrest thresholds in Mode I, and in fact are considerably larger in magnitude.

Crack Propagation Models

Recent micro-mechanical modelling of Mode III fatigue crack growth has been formulated on the premise that Mode III crack advance occurs via the Mode II shear linkage of voids parallel to, and in the immediate vicinity of, the main Mode III crack front (7-9). Although unlikely to be a universal mechanism, this model is consistent with the early work of Tipnis and Cook (50) and with more recent observations on Mode III cracks broken open in liquid nitrogen, where the coalescence of elongated voids can be clearly seen to be confined locally along the main crack front (8).

The proposed mechanism is illustrated schematically in Fig. 16 (7). Micro-mechanical models for this mechanism have been developed based either on considerations of instantaneous crack tip displacement (7,8) or on damage accumulation arguments (8,9). Since for a Mode III crack tip displacement along the length of the void, the Mode III crack will only advance a distance equal to the void width, the models in general predict $(dc/dN)_{III}$ to be a small fraction of the $(\Delta CTD)_{III}$ each cycle, consistent with the experimental results shown in Fig. 3, for example.

As the two models have been described in detail in ref. 8, only a very brief summary is included here. In the crack tip displacement model, growth rates in anti-plane shear are related geometrically to rates of Mode II shear coalescence along the crack front, assuming that crack extension is proportional to the instantaneous ΔCTD. Accordingly, similar to equivalent models for Mode I growth (51), Mode III growth rates are predicted to be dependent upon the first power of the crack tip displacement range, consistent with experimental results in certain materials such as 4340 and 4140 (7,14). Conversely, in the damage accumulation model, the relationship between Mode III crack advance and Mode II shear along the crack front is achieved by assuming that accumulated damage, defined by the Coffin-Manson expression, governs the rate of shear coalescence. Here, Mode III growth rates are predicted to depend upon the crack tip displacement range, raised to the power 1.5, consistent with experimental results in several rotor steels (8,9).

Behavior under Variable Amplitude Loading

The transient growth rate behavior of Mode I cracks subjected to certain variable amplitude loading spectra is now well documented in the literature (e.g., ref. 52). For example, the transient retardations observed following single tensile overloads or high-low block loading sequences have been attributed to crack tip-yield zone interactions, crack tip blunting, crack branching and principally to fatigue crack closure. In Mode III, however, where crack tip

blunting and closure as such do not exist, behavior under variable amplitude loads is very different (9,17).

As illustrated in Fig. 17 for torsional results on A469 rotor steel (9), whereas a single positive overload results in a **retardation** in Mode I growth rates, an initial **acceleration** is observed for Mode III cracks above a 50% overtorque.[3] Similarly, for single fully reversed overloads, Mode III cracks tend to **accelerate** on application of overtorques of 50% or larger, again in contrast to Mode I where a **decelaration** occurs. The response to high-low block loading sequences also is entirely opposite in Mode III compared to Mode I.

As alluded to above, these differences have been attributed to the lack of crack tip shielding mechanisms during Mode III crack extension under variable amplitude loads (9). Whereas following a single overload on a Mode I crack, the "damage" caused by the higher load excursion is more than compensated by concomitant increases in crack tip blunting and crack closure, these mechanisms have little relevance for Mode III cracks. Correspondingly, the "damage" resulting from single overloads simply acceleratates Mode III cracks in accordance with the classical predictions of Miner's rule, without competition from crack shielding mechanisms.

---

[3]The terms overtorque and overtwist are defined as $(\Delta M_o - \Delta M_B)/\Delta M_B$ and $(\Delta\varphi_o - \Delta\varphi_B)/\Delta\varphi_B$, respectively, where ΔM_o and $\Delta\varphi_o$ are the torque and crack mouth rotation at the overload, and ΔM_B and $\Delta\varphi_B$ are the corresponding baseline values.

Summary and Conclusions

Fracture mechanics characterizations of fatigue crack propagation behavior in Mode III (anti-plane shear), specific to damage-tolerant design and lifetime prediction, have important applications in engineering servive, although clearly they are less frequently used compared to corresponding methodologies for Mode I. One such application is in the lifetime prediction of large turbo-generator shafts in electrical power generation and transmission systems, where following particular electrical fault or line switching events, complex high amplitude torsional oscillations can be set up which approach full-scale yielding of the shaft (53). Lifetime prediction procedures have been developed using both fracture mechanics (damage-tolerant) analyses of crack growth (54) and classical stress/life (S/N) curves (55), although in view of the high cost of failure, the inherently conservative nature of the damage-tolerant approach clearly is preferable in this application.

As a basis for such a damage-tolerant analysis of Mode III fatigue, the present article attempts to describe what is currently understood about the mechanics and mechanisms of crack growth in anti-plane shear. It is apparent that to provide a global characterization of Mode III growth rates, similar to the well-known Paris "law" for Mode I fatigue (56), methodology must be developed which both utilizes a characterizing parameter (i.e., "crack driving force") appropriate to large-scale yielding (as Mode III cracking is promoted by extensive crack tip plasticity) and which accounts for

the problem of sliding crack surface interference. In the present approach, the Mode III crack tip displacement, $(\Delta CTD)_{III}$, and plastic strain intensity range, $\Delta\Gamma_{III}$, are proposed as characterizing parameters for Mode III crack extension under large-scale yielding, and experimentally measured growth rates on a range of steels are shown to be proportional to $(\Delta CTD)_{III}$ and $\Delta\Gamma_{III}$ raised to power 1 to 1.5. However, to obtain upper bound data uniquely relating $(dc/dN)_{III}$ to these parameters, allowance must be made for crack surface interference, either by superimposing a small mean tensile load on the cyclic torsional loads or by extrapolating $(dc/dN)_{III}$ vs. crack length data to zero crack length (15).

Micro-mechanical models for cyclic crack advance in anti-plane shear have been described and are found to be consistent with the fractography of Mode III torsional failures. Such models have been applied (9) to Mode III crack growth under variable amplitude loading, where the transient growth rate behavior following single tensile and fully reversed overloads and high-low block loading sequences is found to be completely opposite to that observed for Mode I cracks. Specifically, behavior in Mode III is attributed to the lack of crack tip shielding from blunting and crack closure mechanisms, which results in transient **accelerations** in growth rates, compared to the commonly reported transient **retardations** primarily induced by such shielding mechanisms following overload sequences in Mode I.

Acknowledgements

This review was supported by the Director, Office of Energy Research, Office of Basic Energy Sciences, Materials Science Division of the U.S. Department of Energy under Contract No. DE-AC03-76SF00098. In addition, early Mode III fatigue work was funded by the Division of Energy Conservation, under Contract No. W-7405-ENG-26, Subcontract 9062 from Oak Ridge National Laboratory. While the opinions expressed in the manuscript are idiosyncratic, they result largely from collaborative studies with my colleagues Prof. F. A. McClintock and Dr. E. K. Tschegg and former students, of which Prof. H. Nayeb-Hashemi and Prof. S. Suresh deserve special mention.

References

1. McClintock, F. A., Proceedings of the International Conf. on Fatigue of Metals, Institution of Mechanical Engineers, London, U.K., 1956, p. 538.

2. Hult, J. A., and McClintock, F. A., Proceedings of the Ninth International Congress of Applied Mechanics, Univ. of Brussels, Vol. 8, 1956, p. 51.

3. Hult, J. A., Transactions of the Royal Institute of Technology, Stockholm, Sweden, No. 119, 1958.

4. Kayan, I., Bulletin of the Technical University of Istanbul, Vol. 14, 1961, p. 45.

5. McClintock, F. A., in Fracture of Solids, D. C. Drucker, and J. J. Gilman, Eds., Interscience, New York, TMS-AIME Conf. Ser. 20, 1963, p. 65.

6. McClintock, F. A., and Ritchie, R. O., in Mechanics of Fatigue, T. Mura, Ed., American Society for Mechanical Engineers, New York, AMD-Vol. 47, 1981, p. 1.

7. Ritchie, R. O., McClintock, F. A., Nayeb-Hashemi, H., and Ritter, M. A., Metallurgical Transactions A, Vol. 13A, 1982, p. 101.

8. Nayeb-Hashemi, H., McClintock, F. A., and Ritchie, R. O., International Journal of Fracture, Vol. 23, 1983, p. 163.

9. Nayeb-Hashemi, H., McClintock, F. A., and Ritchie, R. O., Engineering Fracture Mechanics, Vol. 18, 1983, p. 736.

10. Walsh, J. B., and Mackenzie, A. C., Journal of Mechanics and Physics of Solids, Vol. 7, 1959, p. 247.

11. Rice, J. R., International Journal of Fracture Mechanics, Vol. 2, 1966, p. 426.

12. Wright, R. P., and Queeney, R. A., International Journal of Fatigue, Vol. 4, 1982, p. 27.

13. Hurd, N. J., and Irving, P. E., in Design of Fatigue and Fracture Resistant Structures, ASTM STP 761, American Society of Testing and Materials, Philadelphia, PA, 1982, p. 212.

14. Nayeb-Hashemi, H., McClintock, F. A., and Ritchie, R. O., Metallurgical Transactions A, Vol. 13A, 1982, p. 1860.

15. Tschegg, E. K., Materials Science and Engineering, Vol. 54, 1982, p. 127.

16. Tschegg, E. K., Ritchie, R. O., and McClintock, F. A., International Journal of Fatigue, Vol. 5, 1983, p. 29.

17. Nayeb-Hashemi, H., Suresh, S., and Ritchie, R. O., Materials Science and Engineering, Vol. 59, 1983, p. L1.

18. Tschegg, E. K., Journal of Materials Science, Vol. 18, 1983, p. 1604.

19. Tschegg, E. K., Materials Science and Engineering, Vol. 59, 1983, p. 127.

20. Tschegg, E. K., Acta Metallurgica, Vol. 9, 1983, p. 1323.

21. Ritchie, R. O., McClintock, F. A., Tschegg, E. K., and Nayeb-Hashemi, H., in Multiaxial Fatigue, ASTM STP 853, K. J. Miller, and M. W. Brown, Eds., American Society of Testing and Materials, Philadelphia, PA, 1985, p. 203.

22. Ritchie, R. O., International Metals Reviews, Vol. 20, 1979, p. 205.

23. Wulpi, D. J., Metals Progress, Vol. 123, 1981, p. 25.

24. Williams, M. L., Journal of Applied Mechanics, Trans. ASME, Vol. 24, 1957, p. 109.

25. Rice, J. R., Journal of Applied Mechanics, Trans. ASME, Vol. 35, 1968, p. 379.

26. Hutchinson, J. W., Journal of Mechanics and Physics of Solids, Vol. 16, 1968, p. 13.

27. Rice, J. R., and Rosengren, G. R., Journal of Mechanics and Physics of Solids, Vol. 16, 1968, p. 1.

28. Tada, H., Paris, P. C., and Irwin, G. R., in The Stress Analysis of Cracks Handbook, Del Research Corp., Hellertown, PA, 1973.

29. Chitaley, A. D., and McClintock, F. A., Journal of Mechanics and Physics of Solids, Vol. 19, 1971, p. 147.

30. Shih, C. F., Journal of Mechanics and Physics of Solids, Vol. 29, 1981, p. 305.

31. McClintock, F. A., and Tschegg, E. K., International Journal of Fracture, Vol. 26, 1984, p. R11.

32. Erdogan, F., and Sih, G. C., Journal of Basic Engineering, Trans. ASME, Vol. 85D, 1963, p. 519.

33. Gao, H., Alagok, N., Brown, M. W., and Miller, K. J., in Multiaxial Fatigue, ASTM STP 853, K. J. Miller, and M. W. Brown, Eds., American Society for Testing and Materials, Philadelphia, PA, 1985.

34. Pook, L. P., in Multiaxial Fatigue, ASTM STP 853, K. J. Miller, and M. W. Brown, Eds., American Society for Testing and Materials, Philadelphia, PA, 1985.

35. Pook, L. P., and Sharples, J. K., International Journal of Fracture, Vol. 15, 1979, p. R223.

36. Smith, R. A., in Fundamentals of Tribology, N. P. Suh and N. Saka, Eds., M.I.T. Press, Cambridge, MA, 1980, p. 605.

37. Pook, L. P., International Journal of Fatigue, Vol. 7, 1985, p.21.

38. Ritter, M. A., and Ritchie, R. O., Fatigue of Engineering Materials and Structures, Vol. 5, 1982, p. 91.

39. Sudarshan, T. S., Louthan, M. R., and Place, T. A., Materials Science and Engineering, Vol. 66, 1984, p. L27.

40. Suresh, S., and Ritchie, R. O., in Fatigue Crack Growth Threshold Concepts, D. L. Davidson, and S. Suresh, Eds., TMS-AIME, Warrendale, PA, 1984, p. 227.

41. Hourlier, F., McLean, D., and Pineau, A., Metals Technology, Vol. 5, 1978, p. 154.

42. Gross, T. S., Scripta Metallurgica, Vol. 19, 1985.

43. Akhurst, K. N., Lindley, T. C., and Nix, K. J., Fatigue of Engineering Materials and Structures, Vol. 6, 1983, p. 345.

44. Suresh, S., Metallurgical Transactions A, Vol. 14A, 1983, p. 2375.

45. Suresh, S., Vasudévan, A. K., and Bretz, P. E., Metallurgical Transactions A, Vol. 15A, 1984, p. 369.

46. Zaiken, E., and Ritchie, R. O., Materials Science and Engineering, Vol. 70, 1985, p. 151.

47. Dutta, V. B., Suresh, S., and Ritchie, R. O., Metallurgical Transactions A, Vol. 15A, 1984, p. 1193.

48. Minakawa, K., Newman, J. C., and McEvily, A. J., Fatigue of Engineering Materials and Structures, Vol. 6, 1983, p. 359.

49. Zaiken, E., and Ritchie, R. O., Metallurgical Transactions A, Vol. 16A, 1985, p. 1467.

50. Tipnis, V. A., and Cook, N. H., Journal of Basic Engineering, Trans. ASME, Vol. 89, 1967, p. 533.

51. Irving, P. E., and McCartney, L. N., Metal Science, Vol. 11, 1977, p. 351.

52. Suresh, S., Engineering Fracture Mechanics, Vol. 18, 1983, p. 577.

53. Jackson, M. C., Umans, S. D., Dunlop, R. D., Horowitz, S. H., and Parikh, A. C., IEEE Transactions for Power Apparatus and Systems, Vol. 98, 1979, p. 2299.

54. McClintock, F. A., Nayeb-Hashemi, H., Ritchie, R. O., Wu, E., and Wood, W. T., "Assessing Expired Fatigue Life in Large Turbine Shafts," Oak Ridge National Laboratory Report ONRL/Sub/83-9062/1, July 1984.

55. Tanaka, K., Matsuoka, S., Kouzu, F., and Nagata, K., Fatigue of Engineering Materials and Structures, Vol. 6, 1983, p. 103.

56. Paris, P. C., and Erdogan, F., Journal of Basic Engineering, Trans. ASME, Vol. 85, 1963, p. 528.

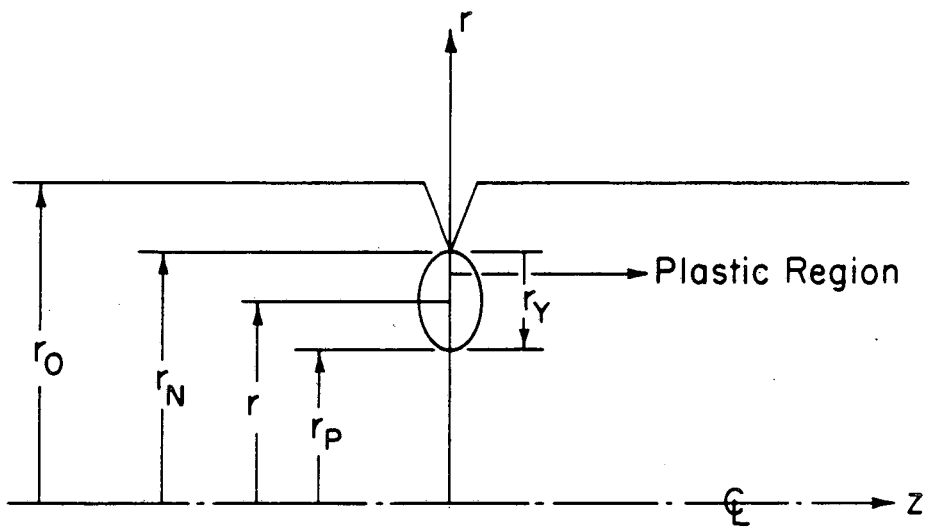

XBL 825-10294

Fig. 1: Nomenclature for plastic zone and respective radii in circumferentially-notched cylindrical torsion specimen.

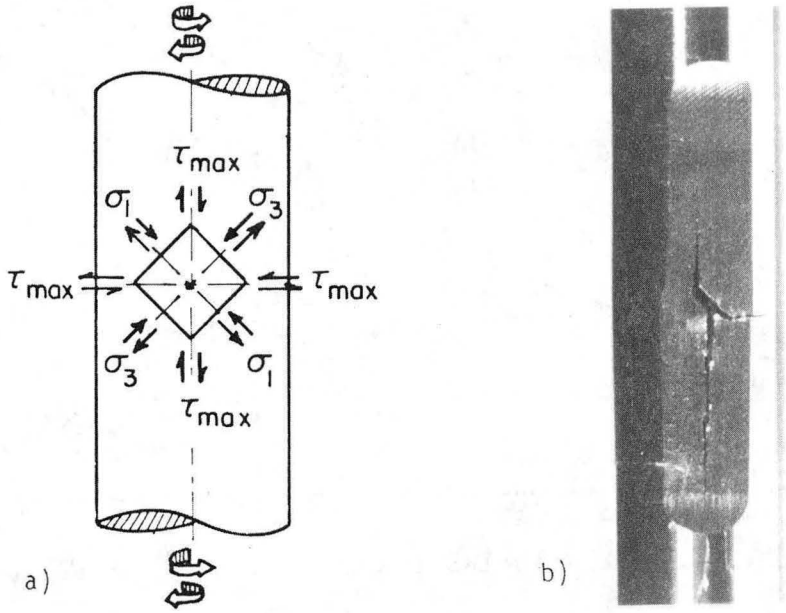

XBB 820-9613A

Fig. 2: a) State of stress and b) longitudinal and radial shear cracks, in a cylindrical bar subjected to cyclic torsion. Shear cracks in A469 rotor steel are Mode II on the surface and Mode III in the interior (courtesy of H. Nayeb-Hashemi).

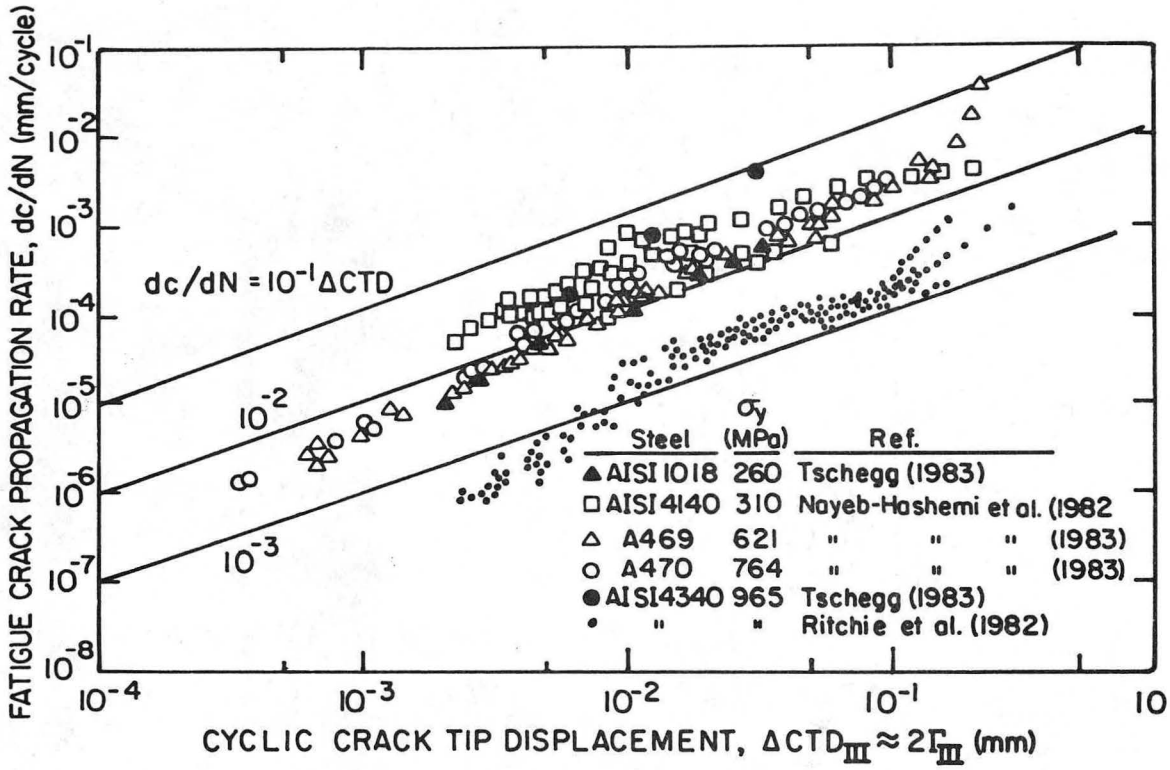

Fig. 3: Mode III fatigue crack growth data, $(dc/dN)_{III}$, plotted as a function of the cyclic crack tip displacement, $(\Delta CTD)_{III}$ $\Delta\Gamma_{III}$, for AISI 1018, AISI 4140, AISI 4340, A469 and A470 steels, after refs. 7,8,14-20. Data (7) for 4340 steel (small symbols) is uncorrected for sliding crack surface interference.

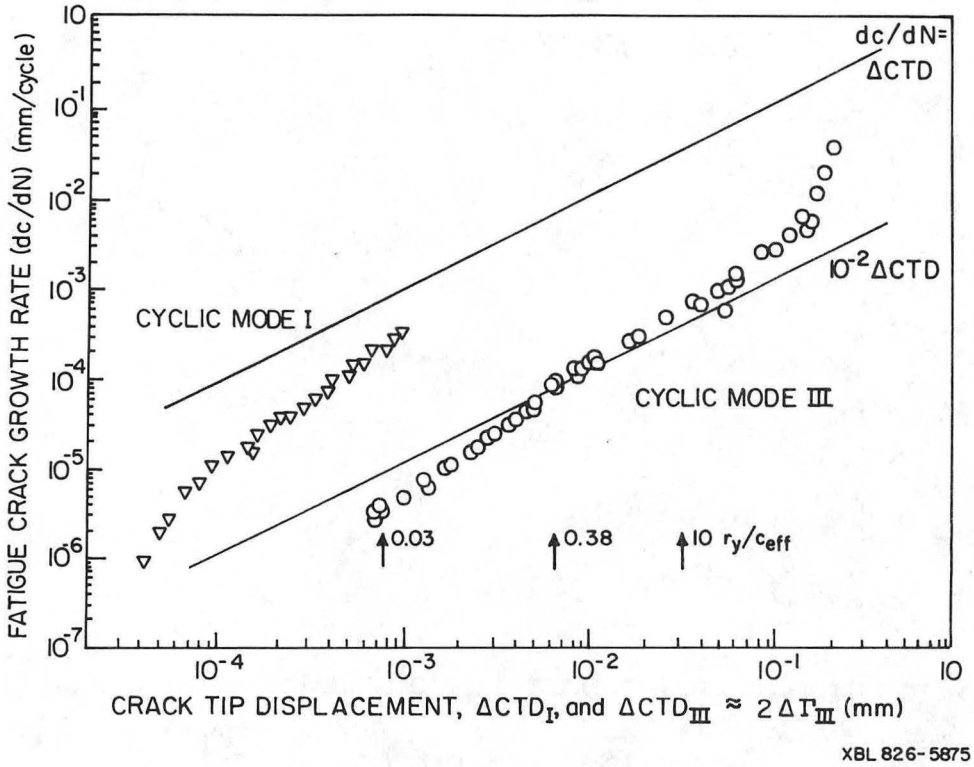

Fig. 4: Comparison of Mode III and Mode I fatigue crack growth rates, as a function of their cyclic crack tip displacements, $(\Delta CTD)_{III}$ and $(\Delta CTD)_I$ respectively, for A469 rotor steel with σ_y = 621 MPa. Mode III results were measured in cyclic torsion with a small superimposed axial load (8).

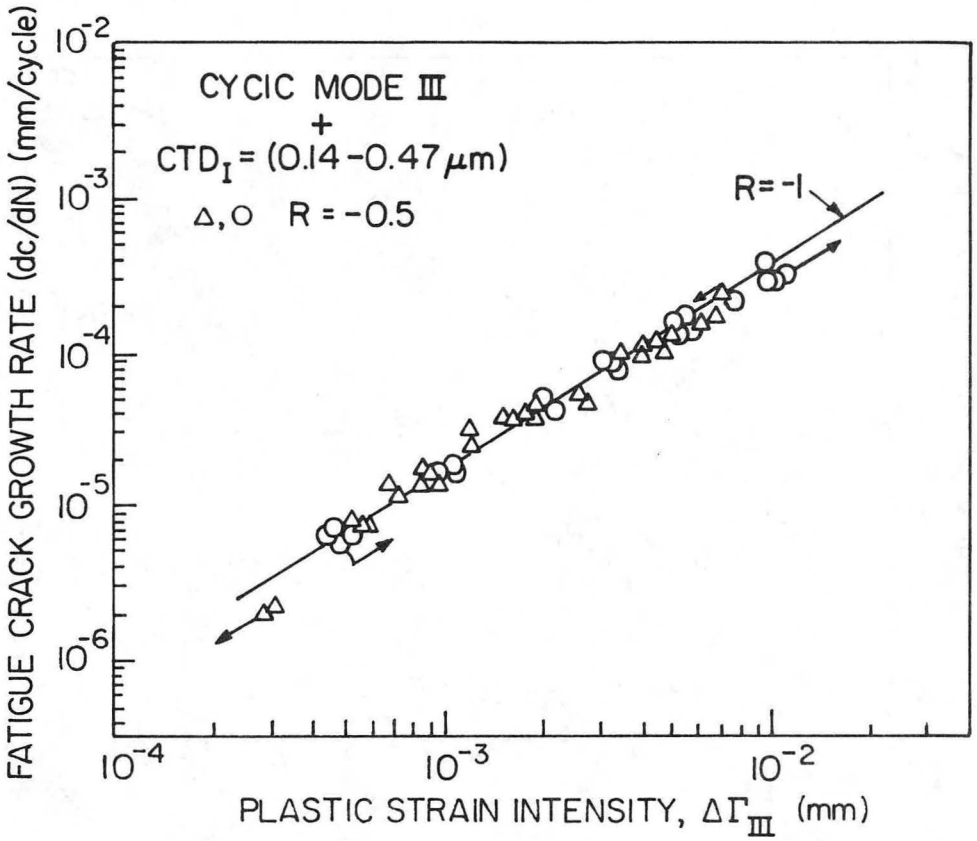

XBL 826-5874

Fig. 5: Influence of load (or stress) ratio R on Mode III fatigue crack growth rates in A469 rotor steel. Data for R = -1 (solid line) and R = -0.5 (data points) were obtained in cyclic torsion with a small superimposed axial load. Arrows indicate direction of crack growth measurements, with Δ denoting decreasing $\Delta\Gamma_{III}$ and ○ increasing $\Delta\Gamma_{III}$ (8).

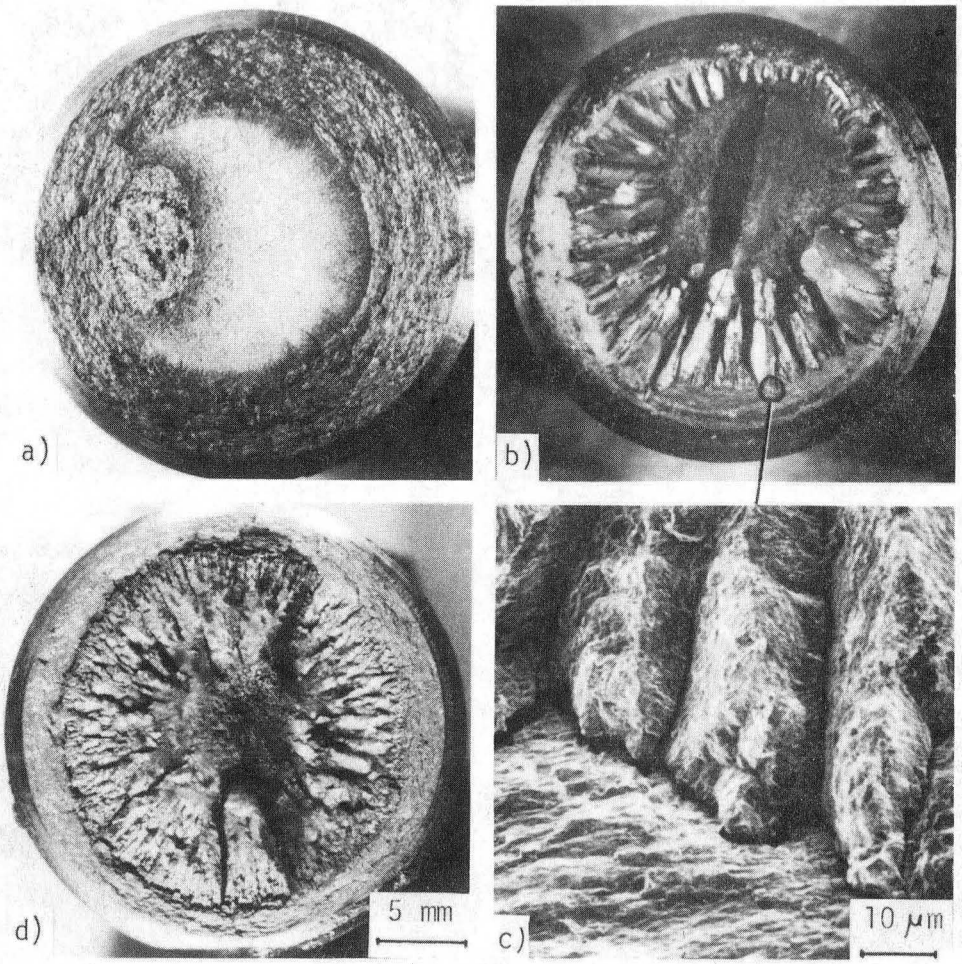

XBB 820-9612

Fig. 6: Survey of torsional fatigue failures (21) showing a) macroscopically flat fracture (true radial Mode III) in 4140 steel at $(\Delta CTD)_{III} \approx 100\text{-}200\ \mu m$ (14), b) "factory-roof" fracture (radial Mode III with 45° Mode I branch cracks) in 4340 steel, c) enlargement of b) at $(\Delta CTD)_{III} \approx 12\ \mu m$ (7), and d) "factory-roof" fracture (radial Mode III with longitudinal Mode III branch cracks) in 4140 steel at $(\Delta CTD)_{III} \approx 6\text{-}120\ \mu m$ (14).

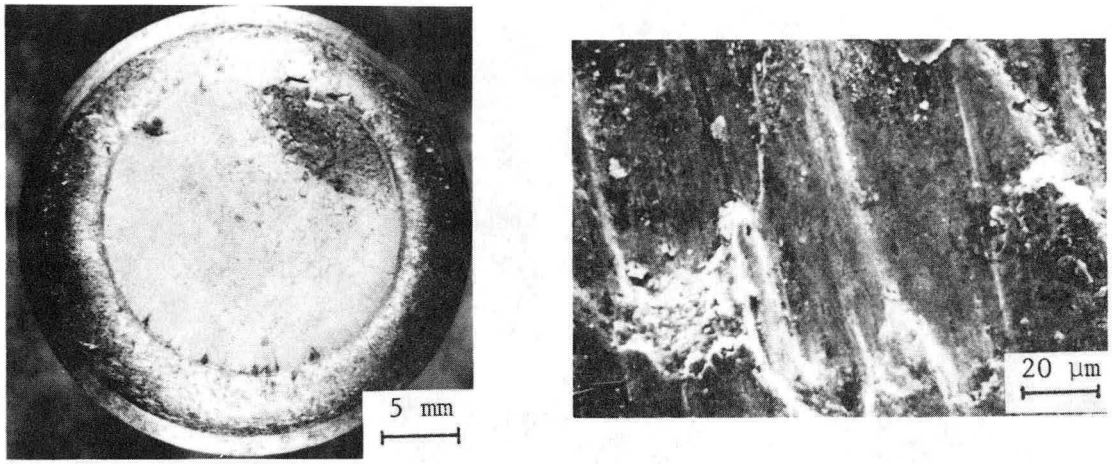

(a)

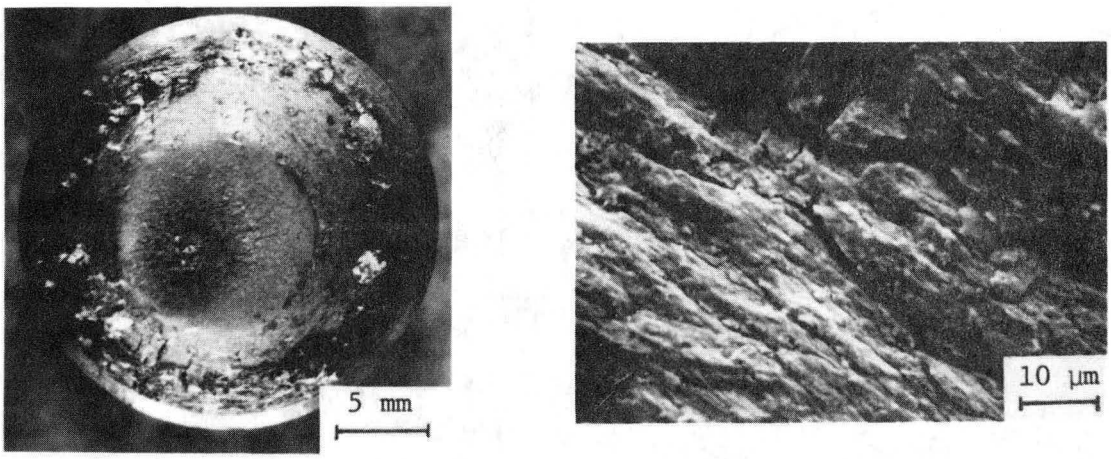

(b)

XBB 856-4993

Fig. 7: Macroscopically-flat true radial Mode III failures in 4340 steel (σ_y = 956 MPa) showing a) abrasion of fracture surface at ΔK_{III} = 25 MPa$\sqrt{m}$ with no superimposed axial load (K_I = 0), and b) decreased abrasion and evidence of secondary branch cracks at ΔK_{III} = 30 MPa$\sqrt{m}$ with superimposed axial load (K_I = 10 MPa$\sqrt{m}$). Arrows indicate general direction of radial crack extension (7).

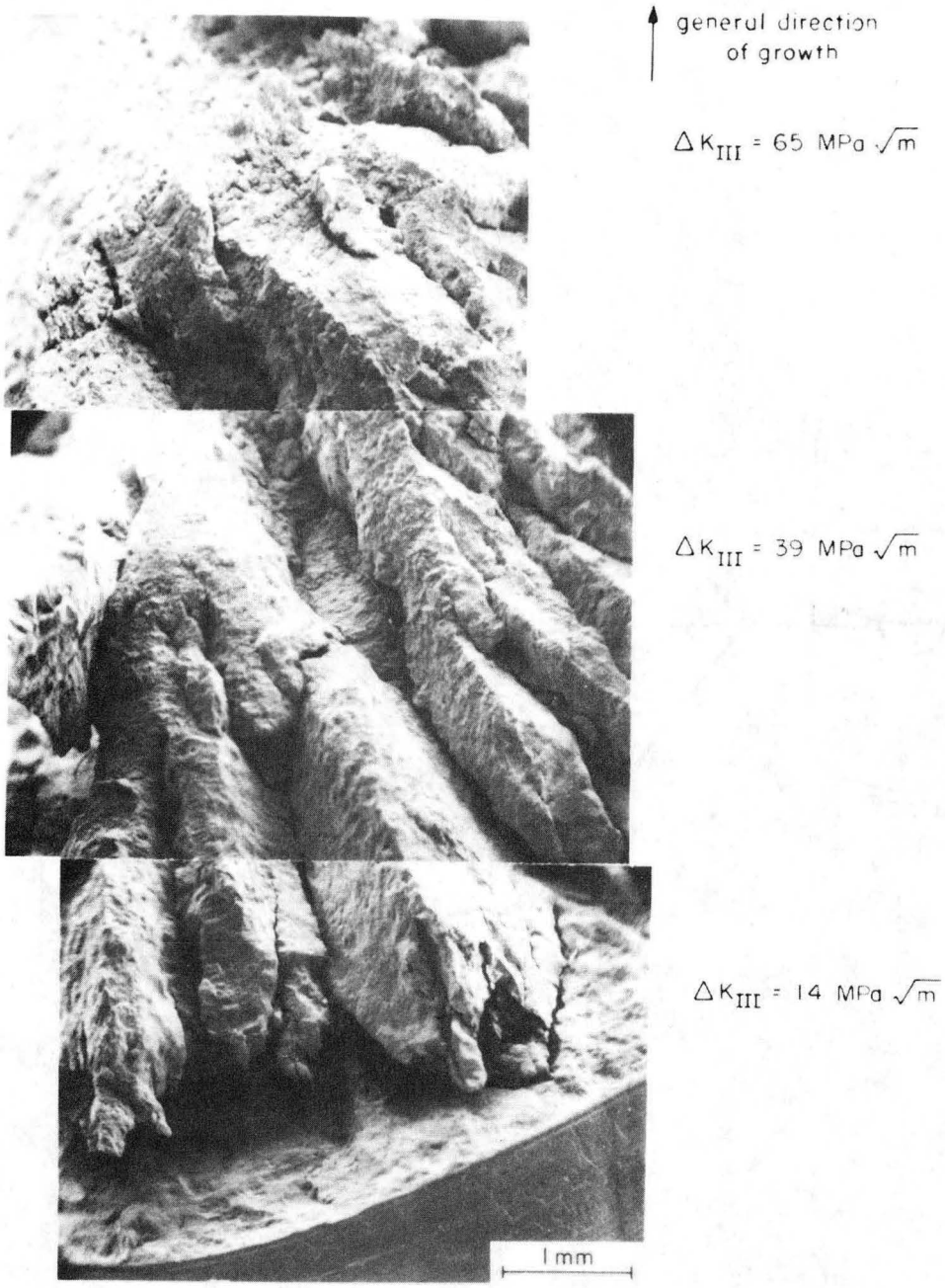

XBB 856-4994

Fig. 8: "Factory-roof" fracture (radial Mode III with 45° Mode I branch cracks) in 4340 steel. Note transition at ΔK_{III} = 14 MPa$\sqrt{m}$ from macroscopically-flat pure radial Mode III fracture (courtsey of H. Nayeb-Hashemi).

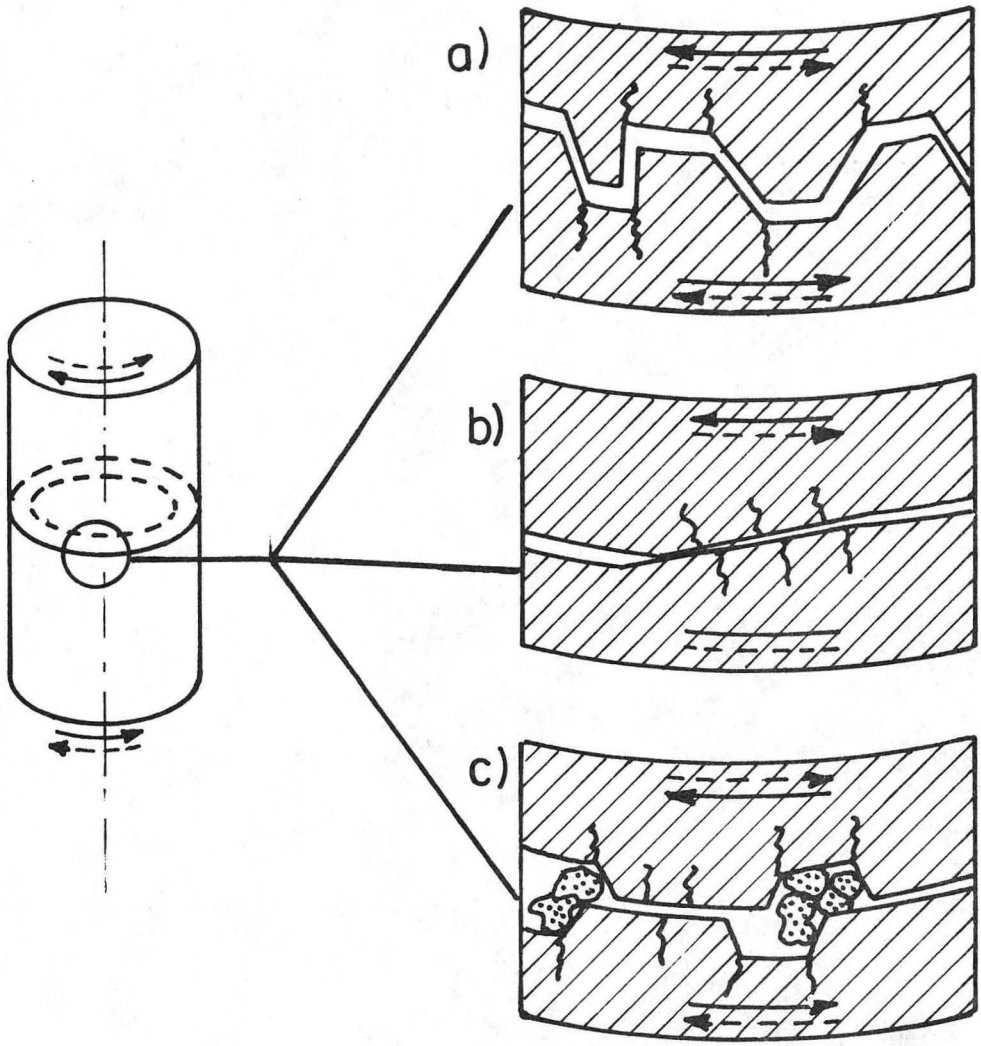

XBL 8210-3149

Fig. 9: Schematic illustration of mechanisms of sliding crack surface interference for Mode III cracks showing a) interlocking of asperities, b) friction and abrasion and c) fretting debris formation (19).

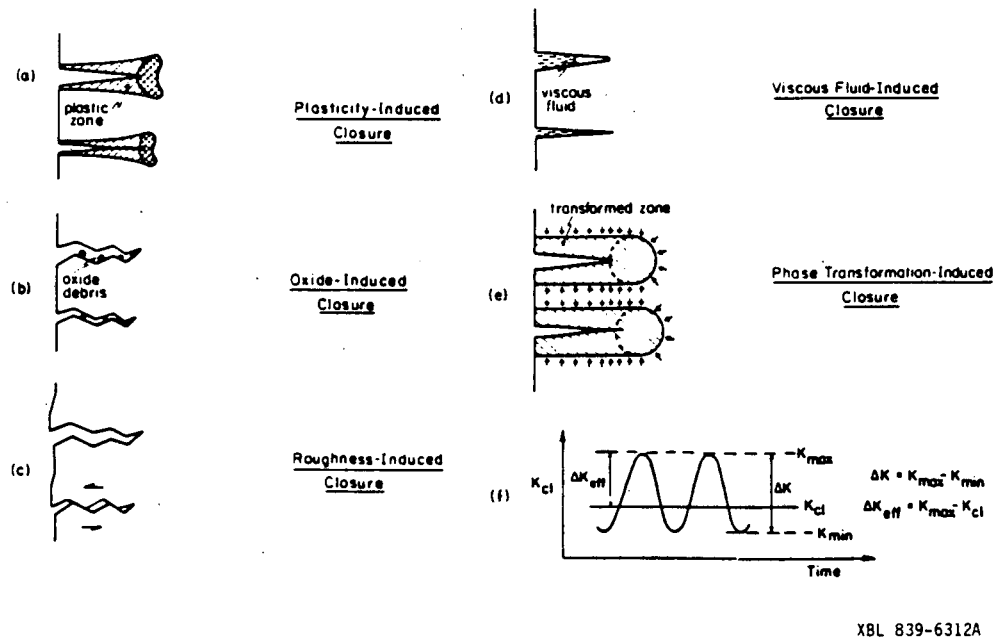

Fig. 10: Schematic illustration of primary mechanisms of crack closure during Mode I fatigue crack propagation (40).

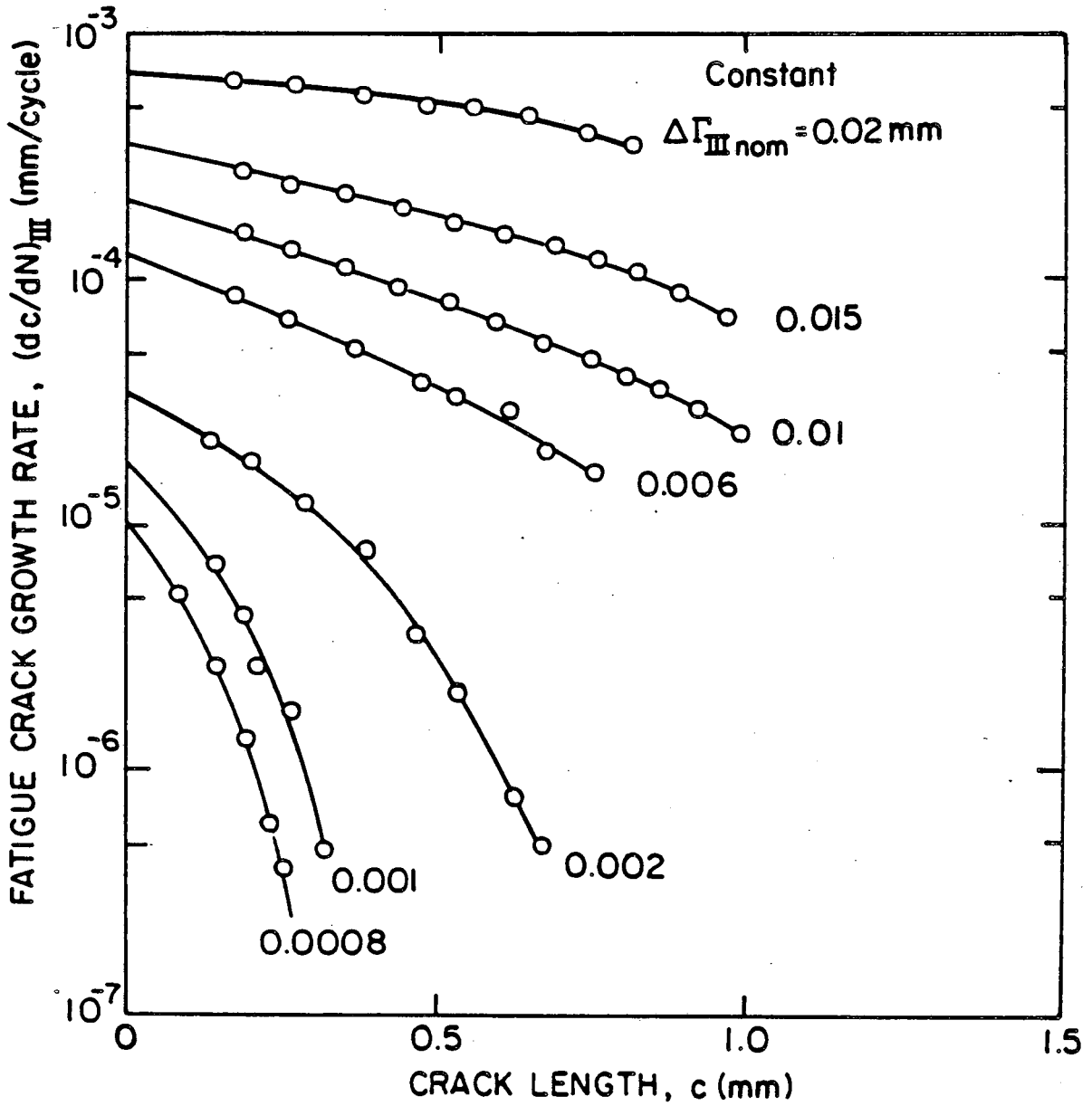

Fig. 11: Mode III fatigue crack growth rates in 1018 steel (σ_y = 260 MPa) as a function of crack length, measured in cyclic torsion at constant nomimal $\Delta\Gamma_{III}$ values. Growth rates are reduced with increasing crack length, particularly at low $\Delta\Gamma_{III}$ levels, due to crack surface interference (after Tschegg (20)).

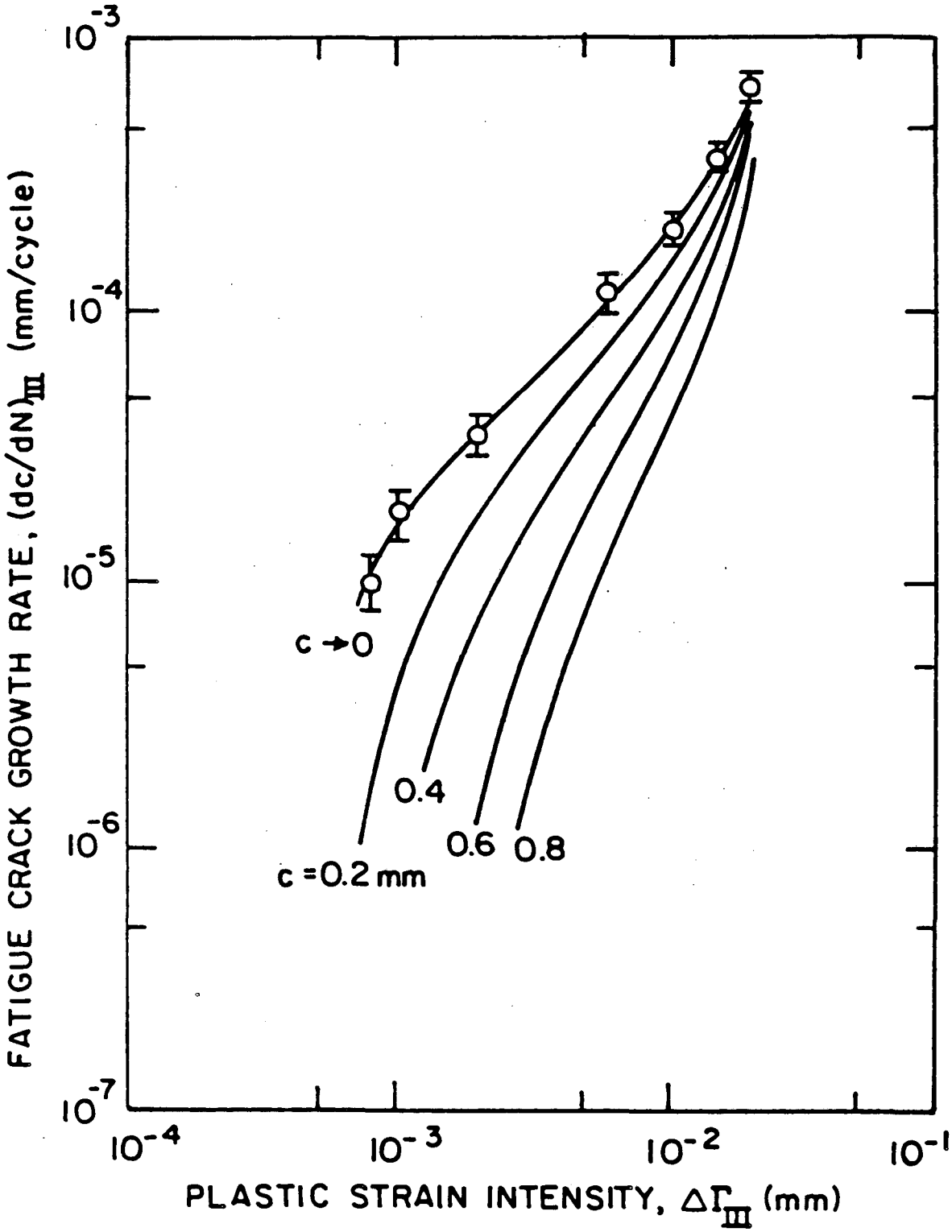

XBL 857-6407

Fig. 12: Variation in Mode III fatigue crack growth rates in 1018 steel with crack length, c, measured from notch. The curve for $c \to 0$ is derived by extrapolating the data in Fig. 11, and is taken to represent behavior in the absence of crack surface interference (after Tschegg (20)).

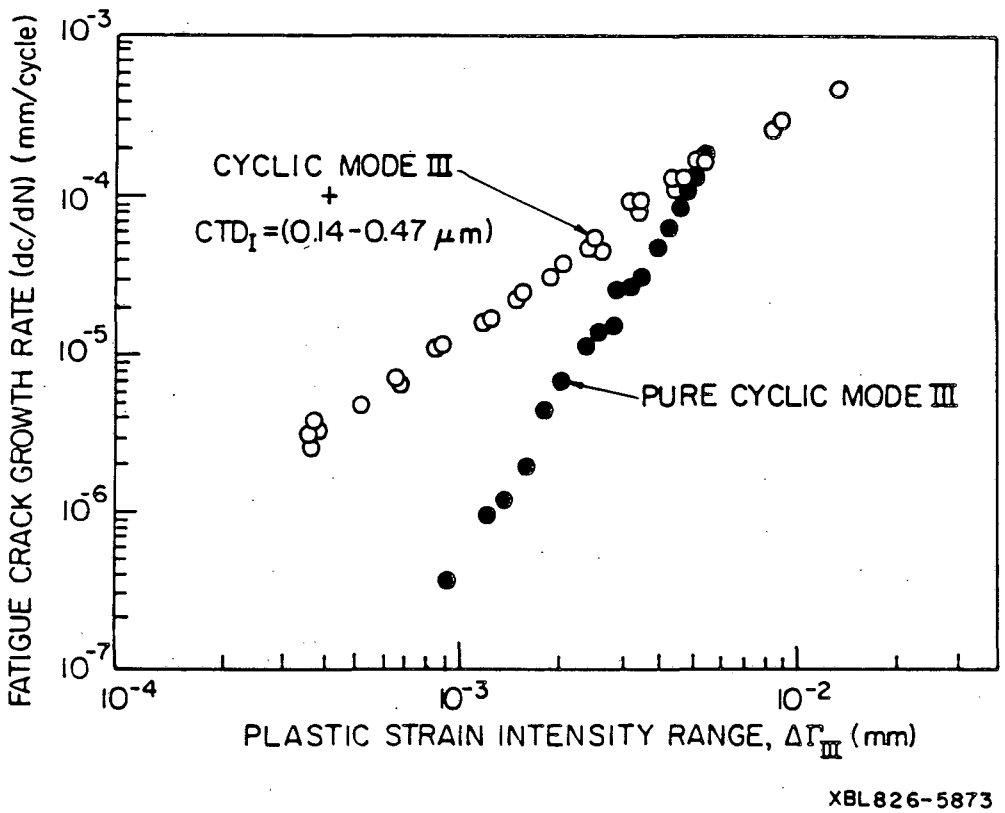

Fig. 13: Comparison of Mode III fatigue crack propagation rates in A469 rotor steel measured in cyclic torsion with and without a small superimposed axial load. Data obtained with superimposed axial load is taken to represent behavior in the absence of crack surface interference (8).

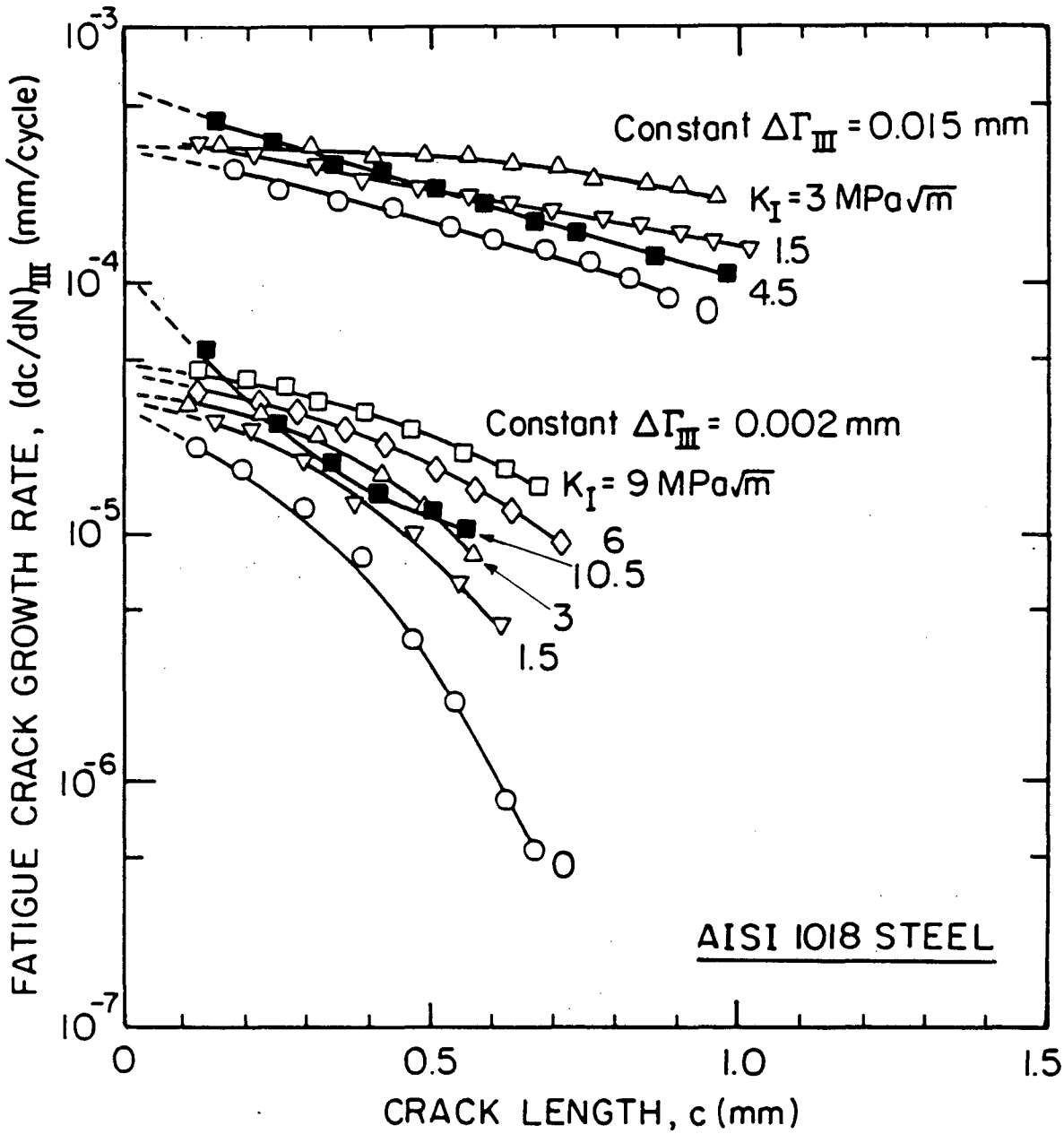

XBL 857-6409

Fig. 14: Influence of superimposed axial load (K_I varying from 0 to 10.5 MPa$\sqrt{m}$) on Mode III fatigue crack growth rates in 1018 steel measured in cyclic torsion at constant nomimal $\Delta\Gamma_{III}$ (after Tschegg (19)).

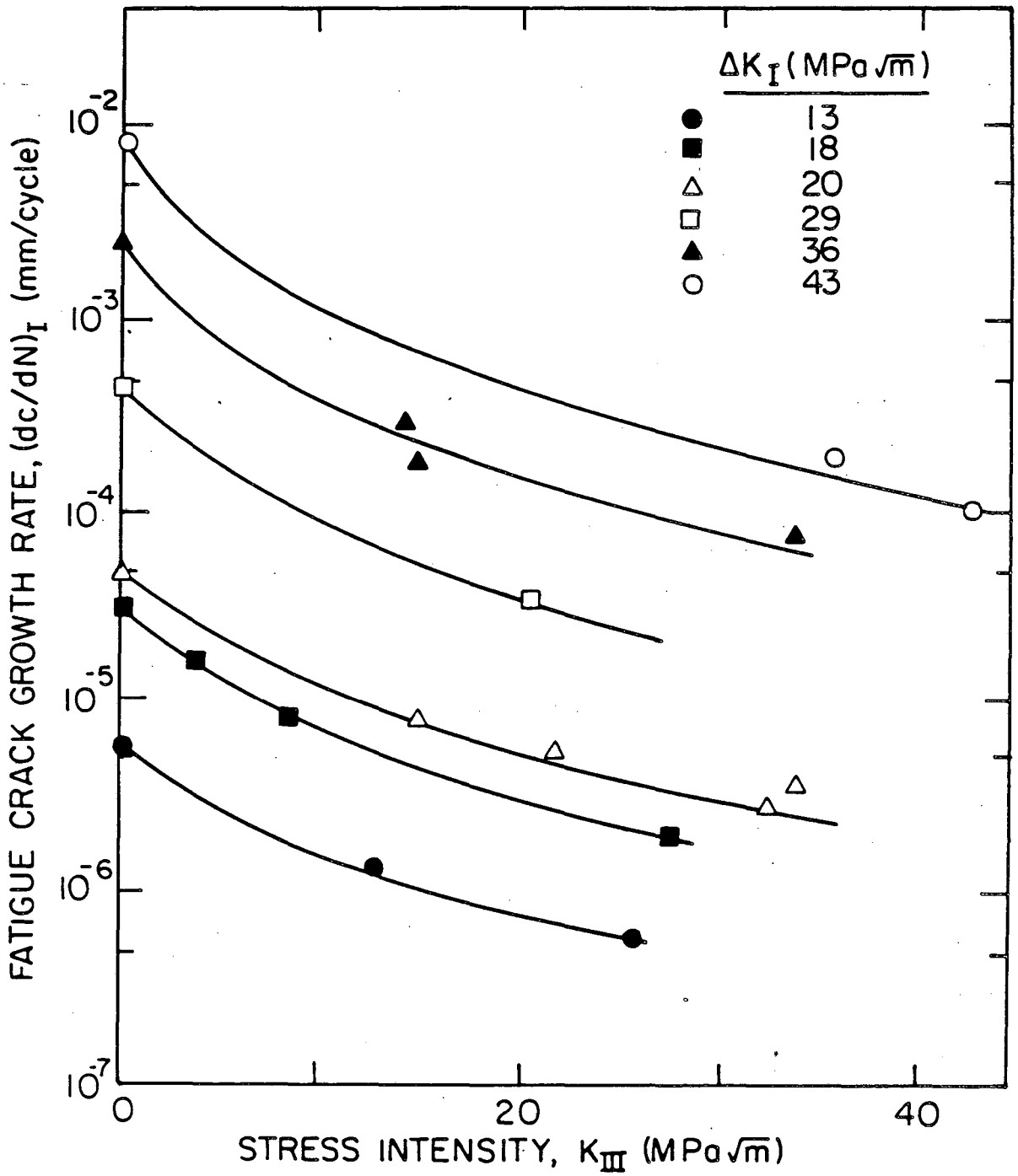

XBL 857-6408

Fig. 15: Influence of superimposed torsional load (K_{III} varying from 0 to 40 MPa$\sqrt{m}$) on Mode I fatigue crack growth rates in Ti-5Al-2.5Sn alloy with σ_y = 760 MPa (after Hourlier et al (41)).

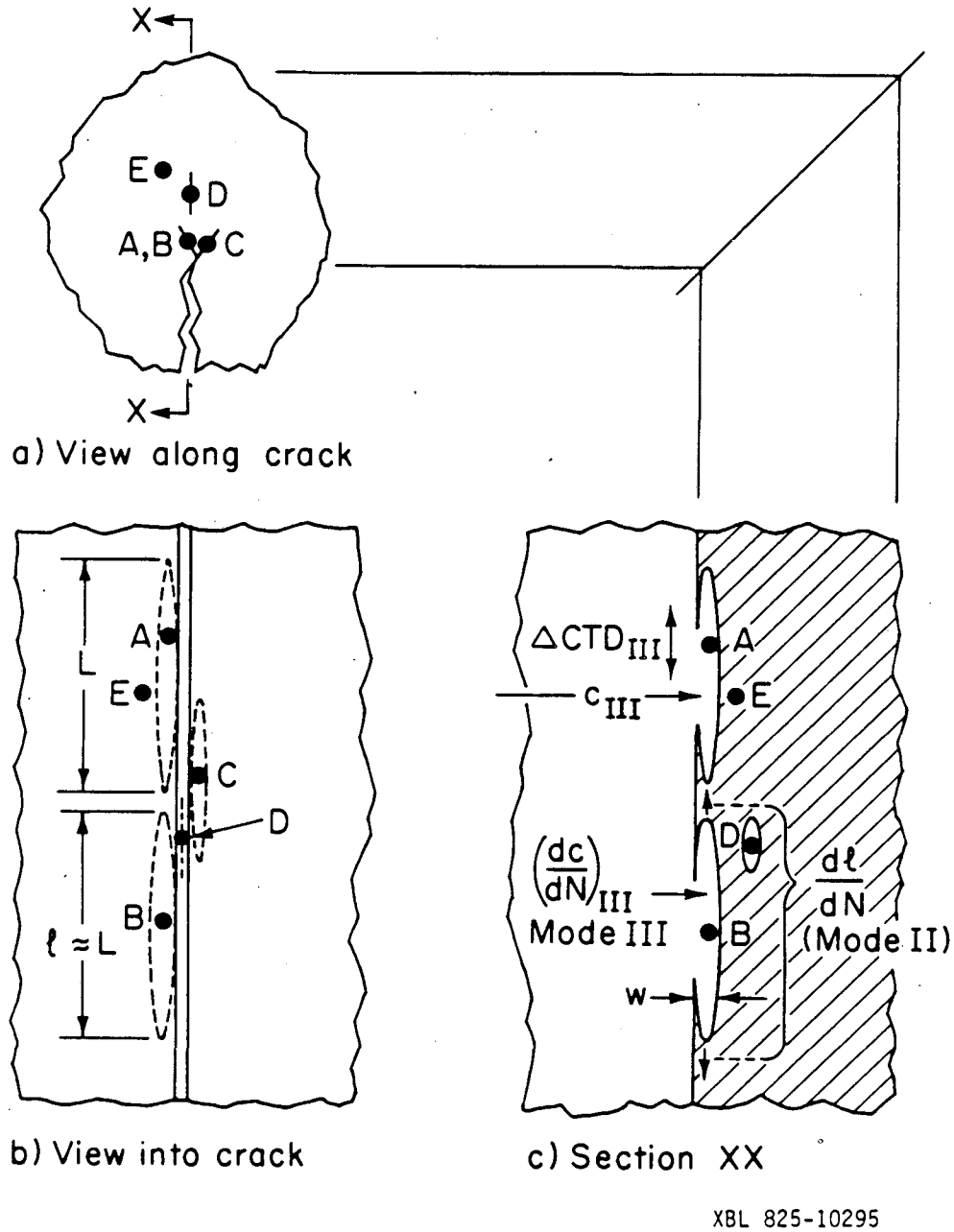

Fig. 16: Schematic illustration of micro-mechanical model for fatigue crack propagation in anti-plane shear showing orthographic views of Mode III crack advance occurring by microscopic Mode II shear along the main Mode III crack front (7).

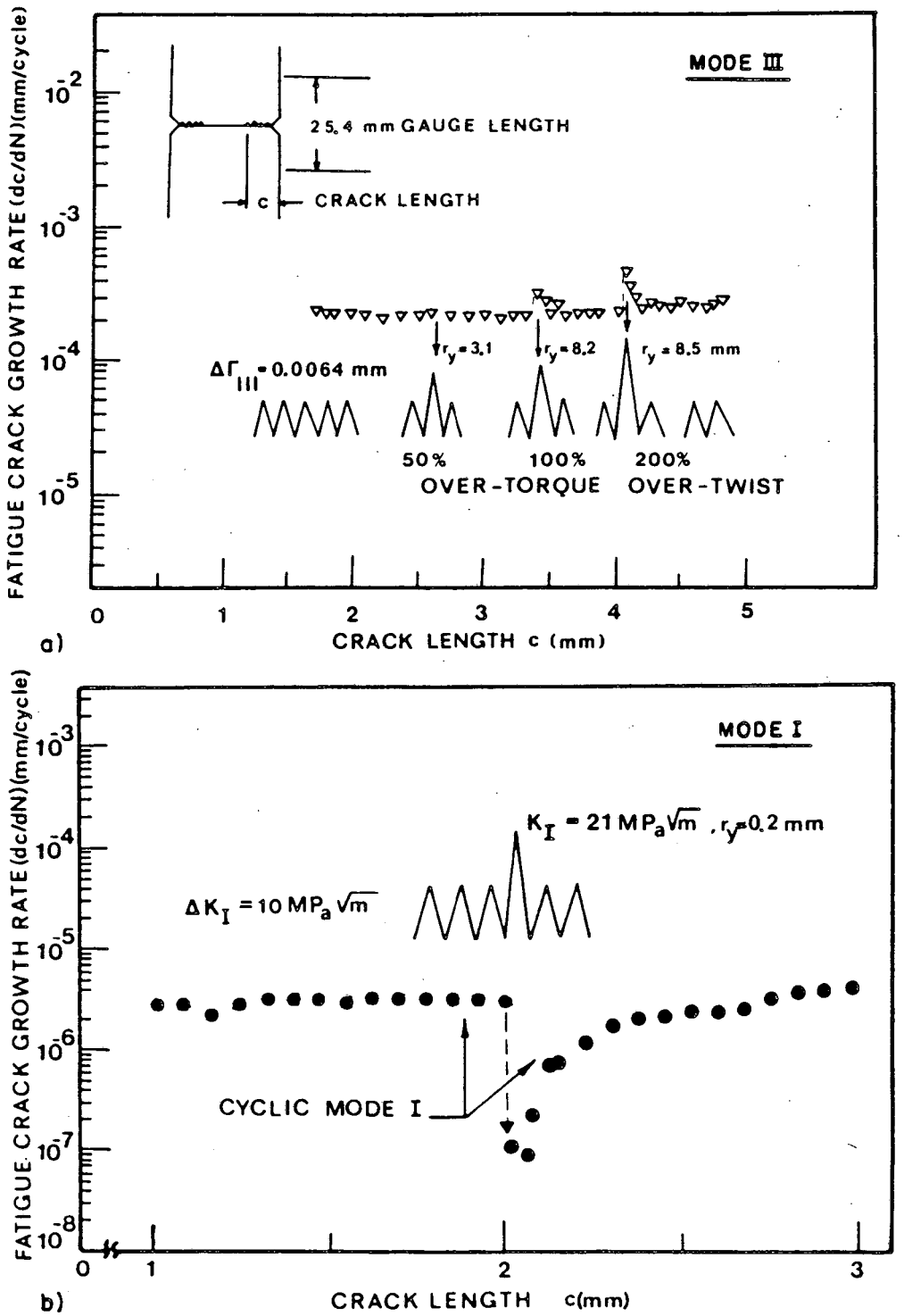

Fig. 17: Comparison of the effect of single (spike) positive overloads on Mode III and Mode I fatigue crack propagation in A469 rotor steel. Note how the transient post-overload response is an acceleration in Mode III compared to a retardation in Mode I (9).

This report was done with support from the Department of Energy. Any conclusions or opinions expressed in this report represent solely those of the author(s) and not necessarily those of The Regents of the University of California, the Lawrence Berkeley Laboratory or the Department of Energy.

Reference to a company or product name does not imply approval or recommendation of the product by the University of California or the U.S. Department of Energy to the exclusion of others that may be suitable.

LAWRENCE BERKELEY LABORATORY
TECHNICAL INFORMATION DEPARTMENT
UNIVERSITY OF CALIFORNIA
BERKELEY, CALIFORNIA 94720